Published in IET Power Electronics
Received on 1st December 2012
Revised on 12th April 2013
Accepted on 11th May 2013
doi: 10.1049/iet-pel.2013.0046

ISSN 1755-4535

Support vector regression-based distortion compensator for three-phase DC–AC boost-inverters: analysis and experiments

Bahman Eskandari, Mohammad Tavakoli Bina
K. N. Toosi University of Technology, Tehran, Iran
E-mail: eskandari@ieee.org

Abstract: Distortion existence in output of power electronics DC–AC converters is inevitable. The amount of distortion in boost-type converters is higher than other types, which is difficult to mitigate. This study introduces a new modification of three-phase boost-inverters in order to mitigate excessive distortions. The compensation process is modified to take advantage of non-linear operation of boost converters and a differential connection of DC–DC converters is employed. Considering DC–AC boost-inverter, it is shown that the outcomes are usually different from the expected desired waveforms. This is because of the non-linear structure of the switching converter. Thus, a compensation method based on support vector regression (SVR) is proposed in a way that the desired waveforms appear at the output of the converter. Analysis and simulations are first introduced for defining the limitations of a boost-inverter because of the non-linear structure. Then, the simulated SVR applied to the external-layer control, comparing the effects of the suggested algorithm with those of the uncompensated cases. Furthermore, practical verification is taken place on an implemented 500 VA boost-inverter in order to confirm the proposed technique as well as theoretical analysis and simulations. The proposal is particularly useful when considering high penetration of inverter-based interfaces for renewable energy sources such as solar panels.

1 Introduction

The power electronic converters play an important role in many applications. In particular, the DC–AC converters are used in applications such as photovoltaic (PV) systems [1–4], uninterruptable power supplies and so on. Let us consider a PV system, with fixed magnitude and frequency, which can be utilised independently or in connection with a grid for power exchange. Thus, the needed converter has to boost the generated voltage by the PV and then convert it to AC (alternatively the AC output could be boosted). These two tasks (booster and DC–AC conversion) are controlled independently; each creates its own power losses. Surveying literatures shows some suggestions on combining these two independent controlled tasks, proposing topologies that perform simultaneously both the DC voltage level and DC/AC conversion [5]. The question, however, is that how the switching pulses should be arranged to generate a sinusoidal output voltage. In fact, the combined topology of these power circuits consists of three DC–DC boost converters (see Fig. 1*a*) that are to deal with high amplitude 50/60 Hz time-variant waveforms. Choosing suitable inductance and capacitance for the boost circuit is difficult because of the time-varying characteristic. In addition, copper losses of the inductor winding severely reduce the gain of the boost converter, especially in big duty cycles [6]. Various modulating techniques were suggested for these combined converters in order to generate sinusoidal waveforms; for example, using adaptive control based on the state space equations [7–10]. Although these complicated control techniques disregard the differential boost structure, this research intentionally concentrates on the differential structure in order to improve the performance in general.

This paper starts with an ideal differential boost-inverter, suggesting a simple formulation of pulse widths for generation of sinusoidal waveform. Then, copper loss of the inductance is taken into account to work out pulse widths in a more realistic state. Despite some improvements on the waveforms, still the output voltage is distorted. It is notable that even PI-controllers followed by various modulating techniques still lead to distorted output voltage because of the non-linear structure of converter. Further, to overcome the stated issue, a compensating technique is introduced based on the support vector regression (SVR) that enables the converter to create sinusoidal waveform. Also, it is suggested that the SVR-based technique can be applied to other converters in order to produce even much better quality waveforms. To assess the proposed solution, first the boost-inverter was simulated; simulation of the SVR-based compensation shows significant improvements compared with those of the uncompensated case. To put the suggestions on a firmer basis, a 500 VA boost-inverter were implemented. Practical outcomes verify the suggested compensating algorithm, demonstrating the capability of the proposal to be applied in practice.

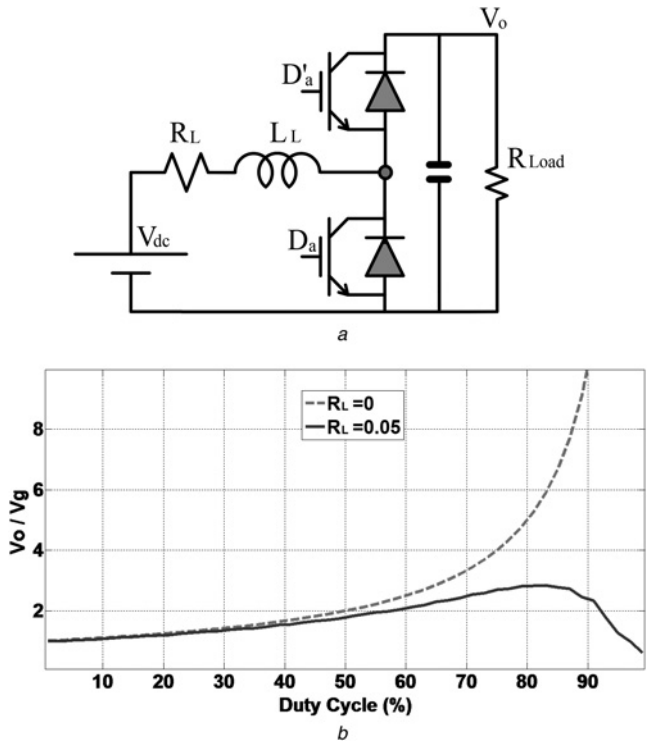

Fig. 1 *A conventional DC–DC boost converter*

a Simple DC/DC boost circuit diagram
b Comparing ideal characteristic of the boost with that of the non-ideal

2 Non-ideals of power electronics converters

Starting from a simple DC–DC boost-inverter, Fig. 1 compares the ideal characteristic with that of the copper losses included. It is evident that the resistance of the inductor has a dramatic influence on the conversion ratio of the boost under high duty cycles [11]. Conventionally, cascading two buck converters in differential connection mode is used very commonly because of the linear gain of the buck (controlled by the duty cycle) that reduces distortion of the output voltage. However, considering the non-ideal characteristic of the boost in Fig. 1*b*, a differential boost-inverter in Fig. 2 cannot easily generate sinusoidal voltage because of its non-linear dependence not only on the duty cycle but also on the load current as well as the inductor resistance. These examples show that achieving ideal sinusoidal output is practically inaccessible because of unavoidable parasitic resistances as well as switching effects. Even under very optimal design conditions, theoretical analysed output is unreachable. To put the subject on a firmer basis, a three-phase differential boost-inverter is implemented according to Fig. 2 in which the discussed matter can be fully inspected.

2.1 Differential pulse-width modulation technique for the three-phase boos-inverter

Assume the principal goal is to build up three phase-to-phase independent sinusoidal voltages at the load terminal of Fig. 2. It is obvious that the gain of the boost converter starts from one when all the controllable switches are always off. Thus, each phase of the boost-inverter in Fig. 2 has a DC offset with respect to the negative pole of the battery ($V_{a\mathrm{N}}$, $V_{b\mathrm{N}}$ and $V_{c\mathrm{N}}$). Based on the gain of an ideal DC–DC boost

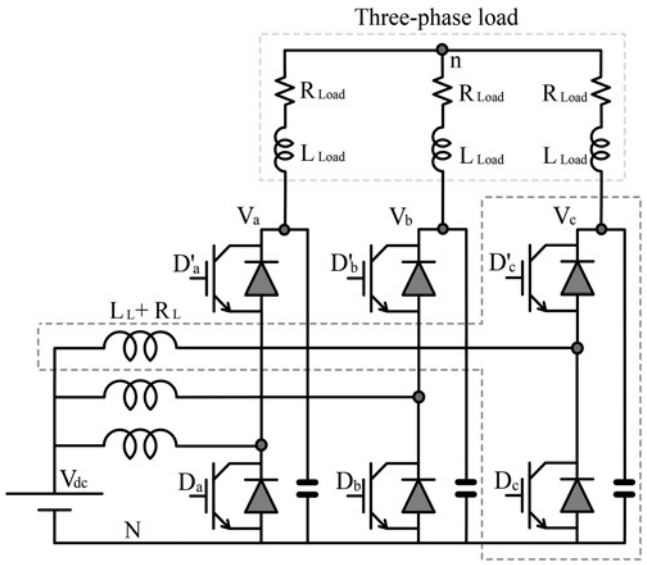

Fig. 2 *Three-phase differential boost-inverter*

converter; assume these voltages are modulated with the following duty cycles as follows

$$\begin{cases} V_{a\mathrm{N}} = \dfrac{V_{\mathrm{dc}}}{1-D_a} = A\sin(\omega t) + A + V_{\mathrm{dc}} \\ V_{b\mathrm{N}} = \dfrac{V_{\mathrm{dc}}}{1-D_b} = A\sin(\omega t + 120^\circ) + A + V_{\mathrm{dc}} \\ V_{c\mathrm{N}} = \dfrac{V_{\mathrm{dc}}}{1-D_c} = A\sin(\omega t + 240^\circ) + A + V_{\mathrm{dc}} \end{cases} \quad (1)$$

where D_a, D_b and D_c are duty cycles for the three legs, V_{dc} is the DC offset of each boost-inverters (that is the amplitude of the input source), and A is the amplitude of the sinusoidal voltages. Note that the boost-inverter voltages have always the same sign as V_{dc}; hence, A has to be added to keep this necessary condition.

By differentiating any two boost voltages in (1), the line voltages of the load are obtained as follows

$$\begin{cases} V_{ab} = V_{a\mathrm{N}} - V_{b\mathrm{N}} = \sqrt{3}A\sin(\omega t - 30^\circ) \\ V_{bc} = V_{b\mathrm{N}} - V_{c\mathrm{N}} = \sqrt{3}A\sin(\omega t + 90^\circ) \\ V_{ca} = V_{c\mathrm{N}} - V_{a\mathrm{N}} = \sqrt{3}A\sin(\omega t - 150^\circ) \end{cases} \quad (2)$$

Therefore the phase-to-neutral voltages at the load are

$$\begin{cases} V_{an} = A\sin(\omega t) \\ V_{bn} = A\sin(\omega t + 120^\circ) \\ V_{cn} = A\sin(\omega t + 240^\circ) \end{cases} \quad (3)$$

These ideal outcomes can be achieved by calculating the three-phase duty cycles using (1)

$$\begin{cases} D_a = 1 - \dfrac{V_{\mathrm{dc}}}{A\sin(\omega t) + A + V_{\mathrm{dc}}} \\ D_b = 1 - \dfrac{V_{\mathrm{dc}}}{A\sin(\omega t + 120^\circ) + A + V_{\mathrm{dc}}} \\ D_c = 1 - \dfrac{V_{\mathrm{dc}}}{A\sin(\omega t + 240^\circ) + A + V_{\mathrm{dc}}} \end{cases} \quad (4)$$

doi: 10.1049/iet-pel.2013.0046

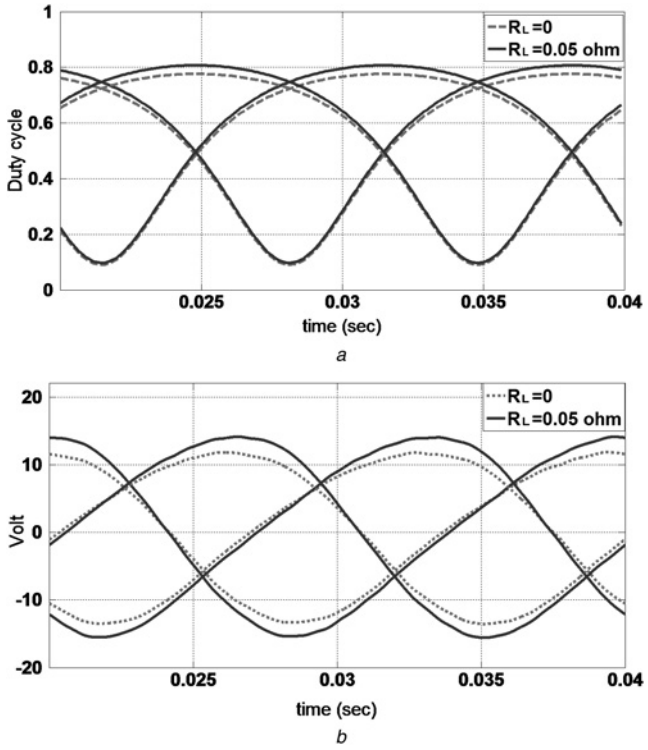

Fig. 3 *Simulated three-phase boost converter*

a Duty cycles excluding ($R_L = 0$)/ including ($R_L = 0.05\ \Omega$) the resistance of the inductor

b Comparing phase-to-neutral output voltages excluding ($R_L = 0$)/ including ($R_L = 0.05\ \Omega$) the resistance of the inductor

In practice, since the inductor's resistance of the boost converter has a large impact on the conversion ratio, (4) is improved by considering the impact of inductor resistance. The proof of (5) is presented in the Appendix (see (5))

To verify and compare (4) with (5) in a three-phase boost-inverter, a series of simulations have been performed using SIMULINK. Fig. 3*a* illustrates calculated duty cycles (D) produced by (4) and (5). Also, the resistance of the inductor makes the duty cycles in (5) different from (4) at high duty ratios. Three phase-to-neutral output voltages of the inverter, as a result of applying (4) and (5), are shown in Fig. 3*b*. The measured THD for these two voltages, modulated by (4) and (5), indicate large quantities of 14.7% and 16.5%, respectively.

2.2 Specifications of the implemented three-phase boost-inverter

A 500 VA, 12 V_{dc}–24 V_{ac}, 50 Hz boost-inverter was implemented according to Fig. 1. This is used as a practical prototype for evaluating the performance of the suggested modulation technique. The power circuit includes a 12 V, 55 Ah batteries as the input dc voltage, V_{dc}, three 200 µH, 10 A inductors, three 250 µF, 100 V capacitors and six IGBT switches (BUP314D). Drivers of the switches are fed through four isolated DC supplies, where the coupler

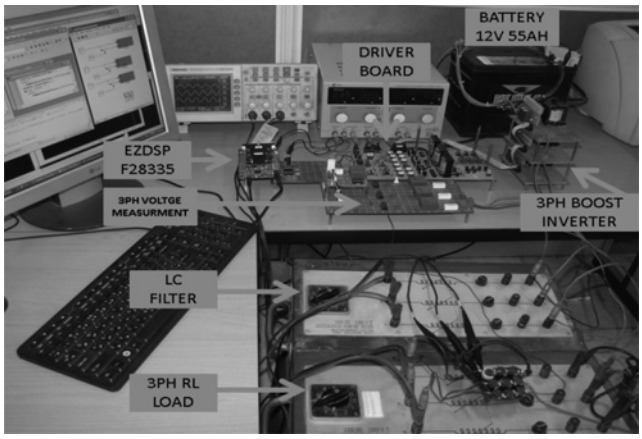

Fig. 4 *Implemented three-phase 500 VA boost-inverter for studying the compensation algorithm*

TLP250 interfaces the microprocessor and the power circuit. A three-phase laboratory L-C set as the output filter and a three-phase laboratory R-L were used as the load. The microprocessor is the EZDSP TMS320F28335 that regulates pulse widths for the six switches using code composer. Fig. 4 shows the implemented boost-inverter described above.

2.3 Uncompensated output voltages of the boost-inverter

The calculated duty cycles, from both (4) and (5) in Fig. 3*a*, were programmed separately with CCSTUDIO on the EZDSPF28335 to drive the six switches of the boost-inverter. Output three phase-to-neutral voltages were recorded by the oscilloscope through serial port for the two uncompensated studied cases; voltage of three phase-to-neutral for each case is shown in Fig. 5*a*. Although the difference between (4) and (5) is considerable, both introduce significant distance from the desired case. It is clear that both output voltages are different from a pure sinusoidal waveform. Even the output voltages contain a DC component. To show the distortion content, Fig. 5*b* depicts the Fourier analysis of both output waveforms. Comparing experiments, the THD obtained by (4) and (5) shows higher harmonic content for (5). Meanwhile, the impact of resistance in (5) can be compensated by increasing the offset A in (4).

2.4 Appling the PI-controller to the boost-inverter

In practice, to reduction the waveform's distortion, one may think of a PI-controller as a regulator of the output voltage of a converter at a certain reference root-mean-sequare (rms) value. This closed-loop PI-controller was also applied to the boost-inverter, both in simulation and practice, where Fig. 6*a* shows the applied PI-loop. Beside the simulations, the implemented boost-inverter was also programmed; the PI-controller was uploaded on the DSP in order to regulate

$$\begin{cases} D_{j=a,b,c}(t) = \dfrac{2m_{j=a,b,c}(t) - V_{dc} - \sqrt{V_{dc}^2 - 4\dfrac{R_L}{R_{Load}} m_{j=a,b,c}(t)^2}}{2m_{j=a,b,c}(t)} \\ m_{j=a,b,c}(t) = A\sin(\omega t + \theta_{j=a,b,c}) + A + V_{dc}\theta = 0^\circ,\ 120^\circ,\ 240^\circ \end{cases} \quad (5)$$

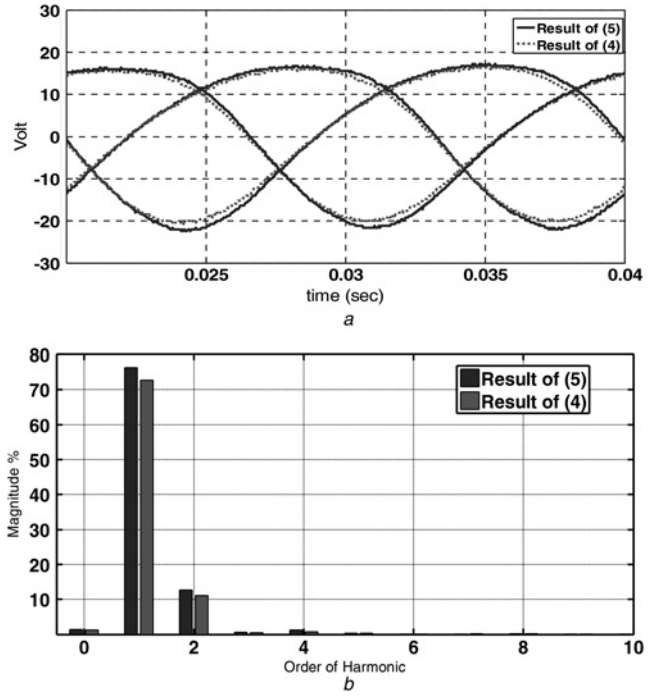

Fig. 5 *Experimental comparison between two introduced modulation techniques (4) and (5)*

a Phase-to-neutral output voltages
b Fourier spectrum

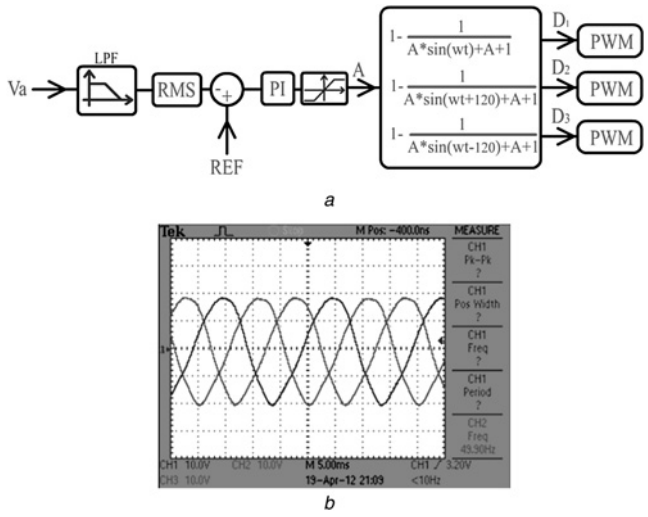

Fig. 6 *Application of the PI controller to regulate the output voltage of boost-inverter*

a Control diagram
b Experimental recorded voltages while both distortion and unbalance peak magnitude still remain in place

the output voltage, Fig. 6*b*. It can be seen that while the output voltage rms value is regulated at 15 V, both distortion and unbalance peak magnitude still remain in place at large.

3 Compensation of non-linear effects of converters

Both simulations and experiments show that uncompensated boost-inverter introduces a distorted output voltage, including unbalance peak magnitude according to Fig. 5. In the meantime, even conventional PI-controller was unable to eliminate unbalance peak magnitude and distortion. One question still remains to be answered; how a desired output can be generated through a switching converter by manipulating its modulated input [12–19]. Before answering this question, let us raise an idea based on the above simulations and experiments. An ideal input, to an ideal converter delivers an ideal outcome. Also, an ideal input to a non-ideal converter provides a non-ideal outcome. Hence, as a preliminary idea, the input to the non-linear converter should be compensated in a way to obtain the desired output. To put the raised idea in practice, the SVR was studied that is briefly described in the following subsection.

3.1 Introduction to the SVR in brief

The field of machine learning is expanding in the last few years, and many new technologies are growing using these principles. Among the various existing algorithms, one of the most recognised is support vector machine (SVM) for classification and SVR, which permit the creation of systems which, after training from a series of examples, can successfully predict the output at an unseen location performing an operation known as induction.

Suppose we are given training data $\{(x_1, y_1),\ldots, (x_N, y_N)\} \subset X \times R$, where X denotes the space of the input patterns (e.g. $X = R^d$). Our goal is to find a function $f(x)$ that has at most ε deviation from the actually obtained targets y_i for all the training data, and at the same time is as flat as possible. The form of estimated function by SVR is

$$f(x,\ \omega) = \omega^T \Phi(x) + b \quad \text{with } \omega \in \mathrm{x},\ \mathrm{b} \in R \tag{6}$$

where the non-linear function $\Phi(x)$ is a mapping from R^d to so-called higher dimensional feature space F, $\boldsymbol{\omega}$ is a weight vector to be identified in the function and b is a bias term. To calculate the weight vector $\boldsymbol{\omega}$, the following cost function should be minimised [20]

$$\text{minimise } Q(\boldsymbol{\omega},\ \xi,\ \xi^*) = \frac{1}{2}|\boldsymbol{\omega}|^2 + \gamma\left(\sum_{i=1}^{N} \varsigma(\xi_i) + \sum_{i=1}^{N} \varsigma(\xi_i^*)\right)$$
$$\text{subject to } \begin{cases} y_i - \boldsymbol{\omega}^T \Phi(x) - b \le \varepsilon_i^* \\ \boldsymbol{\omega}^T \Phi(x) + b - y_i \le \varepsilon_i^* \\ \varepsilon_i,\ \varepsilon_i^* \ge 0 i = 1, \ldots, N \end{cases} \tag{7}$$

where γ is a prespecified value that controls the cost incurred by training errors and the slack variables, ξ_i, ξ_i^*, are introduced to accommodate error on the input training set. With many reasonable choice of loss function, ζ, the solution will be characterised as the minimum of a convex function. Common procedure to solve the (7) is through production of the Kernel function and fined the Lagrange multipliers by using the quadratic-programming [20, 21].

3.2 How to apply the SVR in practice as a compensator

The studied case of three-phase boost-inverter showed that suggested modulation techniques (4) and (5) generated distorted output voltage. To apply the SVR as the compensator, assume there is a relationship between the 'input pulse widths' and 'the output voltage'. Now, if a

doi: 10.1049/iet-pel.2013.0046

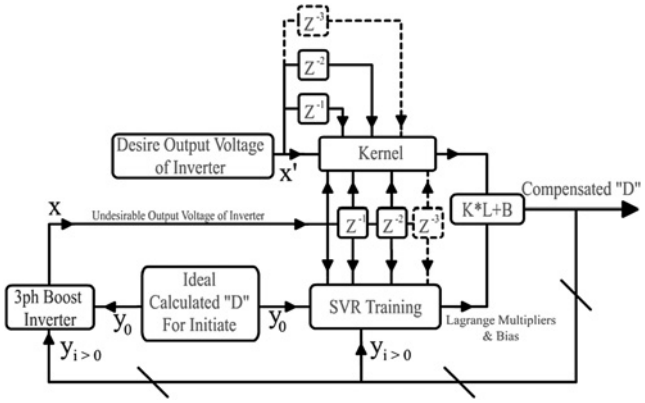

Fig. 7 *Overall suggested procedure for compensating non-linear effects in power electronic converters*

sinusoidal waveform is applied as the input to this relationship, then the output will be the required pulse widths. These resultant pulse widths can be applied to the boost-inverter to obtain the desired sinusoidal output voltage. In fact, one may concentrate on the desired output instead of directly working on duty cycles. To put the SVR in practice, a numerical relationship should be made between input and output data vectors. For example, let the boost-inverter case is operating under the modulation technique either (4) or (5). Since the output voltage is distorted non-sinusoidal (non-ideal output), this case is taken sample for a main cycle of equivalent sinusoidal waveform. Although more number of samples would be precious, the SVR can also relate input and output vectors with lower number of samples suitably. Let the samples of input vector is called $\boldsymbol{X}$ and samples of the output vector $\boldsymbol{Y}$. Then, the SVR relates input to output by means of generating Kernel and finding the Lagrange multipliers. Having obtained this relationship, now the desired output of the boost-inverter (a pure sinusoidal waveform) is given as the second input to the SVR. Then, the output of the SVR will show the required pulse widths or duty cycles. These resultant pulses eventually are applied to the boost-inverter to generate a pure sinusoidal waveform. The whole procedure is shown in Fig. 7. The cycle of compensation starts by feeding $\boldsymbol{Y}_0$ to the boost-inverter. Then, outcomes from the boost-inverter ($\boldsymbol{X}$) are fed to the SVR along with $\boldsymbol{Y}_0$ in order to build up the Lagrange multipliers. At the same time, both $\boldsymbol{X}$ and its desired outcomes $\boldsymbol{X}'$ are used to establish the Kernel [12]. Eventually, both the Kernel and Lagrange multipliers generate the compensated duty cycles. The first compensated duty cycles have to be fed as the new input pattern for the boost-inverter ($\boldsymbol{Y}_1$); for further compensation stages ($i > 1$), however, this optional procedure is decided by the user to recognise the necessity of applying $\boldsymbol{Y}_i$ to the boost-inverter (slashed-mark in Fig. 7).

This can be named as the main feature of the proposed technique in which the compensating process could be reiterated several times by feeding the newly generated data as the input. This iterative process is shown in Fig. 7, where increasing the number of iterations (more than two) enhances the quality of compensation. Meanwhile, it should be noted that both $\boldsymbol{X}$ and $\boldsymbol{X}'$ along with their history (Z^{-1}, Z^{-2},…, Z^{-n}) can be stored as many as required. However, various performed experiments show that increasing the number of historical cycles beyond three has insignificant impact on the quality of the outcomes.

4 Verification of the proposed compensator

To inspect the performance of the proposed compensator, the implemented boost-inverter was modulated with different techniques, and outcomes are compared correspondingly.

4.1 Applying (4) as the modulator to the boost converter

Initially, three inputs are applied to the proposed compensator including the modulator stated by (4) as $\boldsymbol{Y}_0$, the measured output voltages as $\boldsymbol{X}$ and the desired three-phase sinusoidal output voltages $\boldsymbol{X}'$. The proposed compensator provides proper pulse widths as shown in Fig. 7. Fig. 8*a* compares the duty cycles modulated by the uncompensated (4) with those of the described compensating procedure. The resultant voltages of these techniques are compared in Fig. 8*b*. It is clear that the proposed compensator provides closer outputs to those of the ideal case, improving the

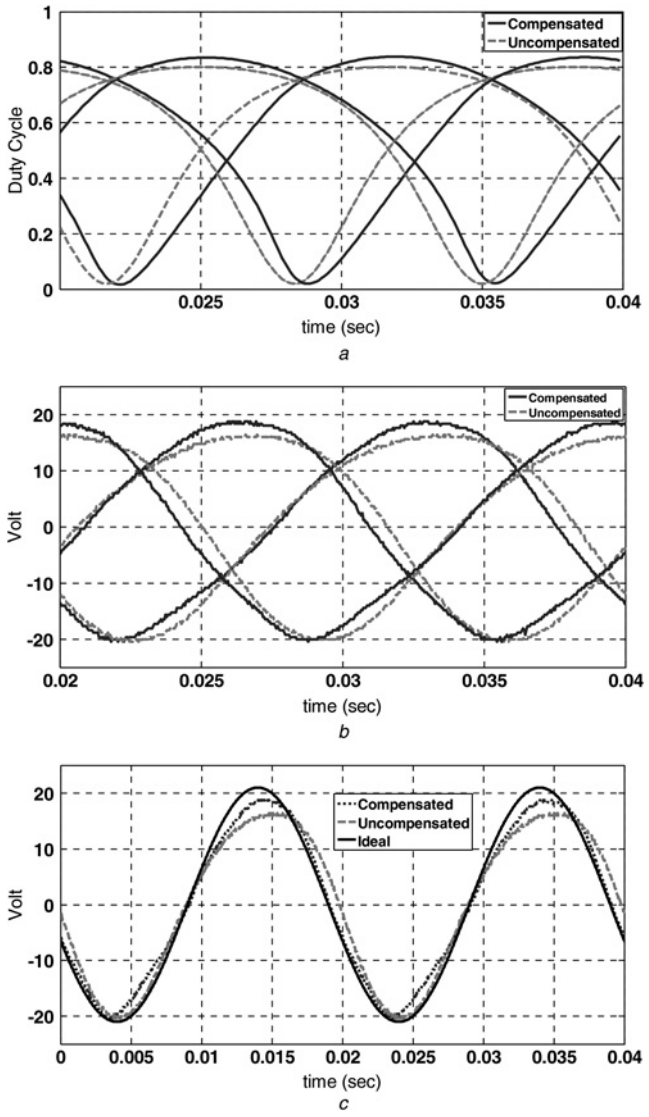

Fig. 8 *Experimental results*

a Comparing duty cycles generated by (4) with those of the proposed compensation technique

b Comparing output voltage produced by (4) with those of the proposed compensation technique

c Comparing generated voltages with that of an ideal sinusoidal voltage

quality of the output voltage significantly under the compensated proposal as shown in Fig. 8*c*.

4.2 Applying (5) as the modulator to the boost-inverter

Similarly, the uncompensated modulation (5) can be compared with that of the proposed compensator as illustrated in Fig. 9. Comparing Figs. 8*b* with 9*b*, it can be observed that inclusion of the resistance of the inductor has little impact on improving the quality of the output waveforms. In fact, other non-ideal factors such as voltage drop on diode and IGBT, resistance of capacitor and dead time in particular is excluded from (5). Thus, the main advantage of the proposed compensator is its independence from the undetermined parameters of the circuit in the compensation process.

4.3 Consecutive compensations

One significant advantage in the proposed compensation technique is the possibility of consecutive application of the resultant duty cycles to the SVR. In other words, a compensated system can be improved further by re-compensation. To achieve this purpose, the compensated outputs (see compensated duty cycles in Fig. 7) have to be taken sample again, and fed as a new input to the SVR. Consecutive compensation process has been repeated up to five times on the implemented boost-inverter. The best results were obtained from the second iteration. If the number of consecutive compensations is increased beyond two, then significant drop is observed in the quality of output voltages of the boost-inverter. Fig. 10 shows the results of two consecutive compensations.

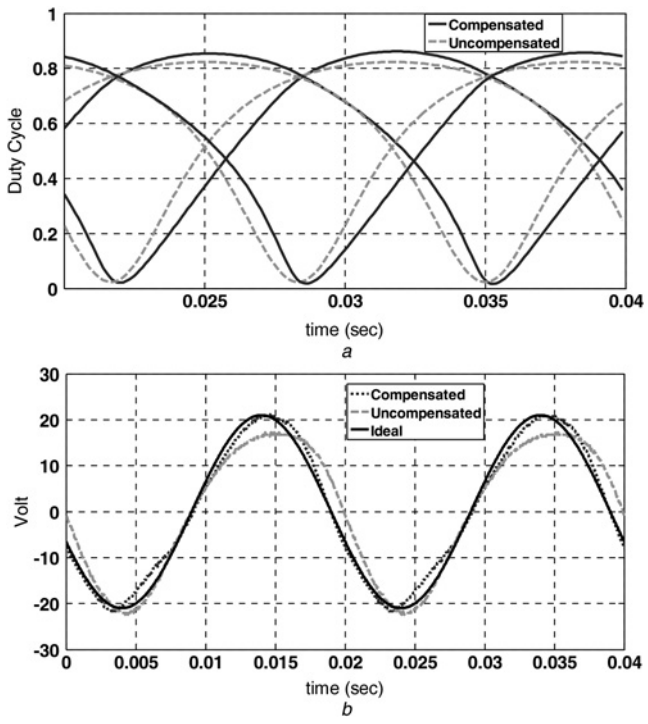

Fig. 9 *Experimental results*

a Comparing duty cycles generated by (5) with those of the proposed compensation technique
b Comparing generated voltages with that of an ideal sinusoidal voltage

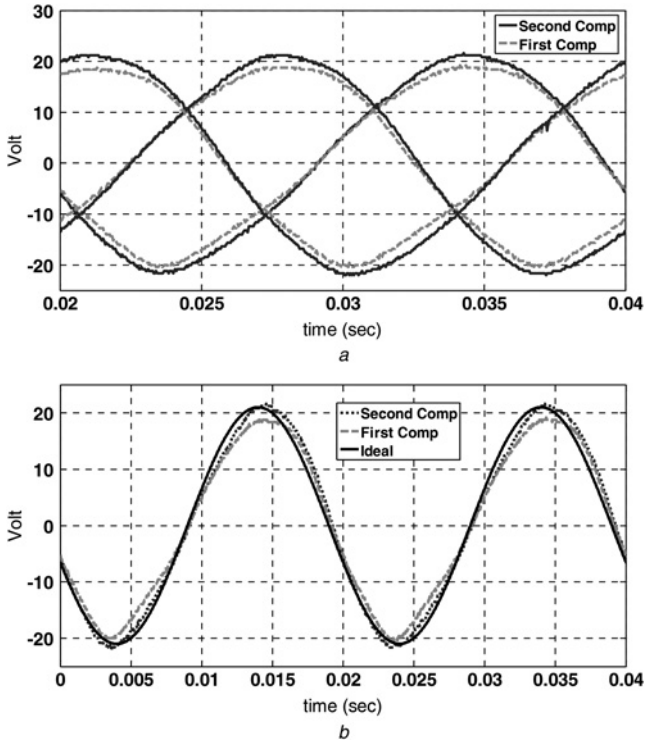

Fig. 10 *Experimental results*

a Comparing output voltages generated by once and twice compensations
b Comparing compensated voltages with that of an ideal sinusoidal voltage

4.4 Harmonic analysis

Here harmonic spectra are compared for all three discussed experiments as shown in Fig. 11. The results indicate that twice consecutive compensation introduces the best THD for the output voltages of the boost-inverter, having the biggest fundamental component along with the smallest harmonics. Table 1 compares the THD of the output voltages both for simulations and experiments, verifying the proposed compensation approach.

In brief, a designed three-phase boost-converter, uploaded with the suggested compensator, has the following advantages and benefits in comparison with conventional converters (multi-stage converters (DC/DC along with DC/AC) as follows:

- The compensated boost-converter provides both 'DC/AC conversion' and 'voltage boost' all in a single-stage. This is cheaper and more compact than conventional multi-stage converters, associating with neither switching devices with reverse voltage blocking capability nor power transformers.
- There are no appropriate approaches for utilising uncompensated three-phase boost-inverters because of highly distorted output voltage.
- Output voltages of three-phase boost-inverters are conventionally compensated by various approaches such as usual PI-controllers and advanced sliding-mode controllers (e.g. [3, 5]); but, the output voltages still remain highly distorted.
- The SVM-compensated three-phase boost-inverter is simpler and more affordable in comparison with classical multi-stage converters.

5 Online look-up table compensation

The compensating procedure (Fig. 7) is an off-line process, whereas the boost-inverter has to be modulated online

doi: 10.1049/iet-pel.2013.0046

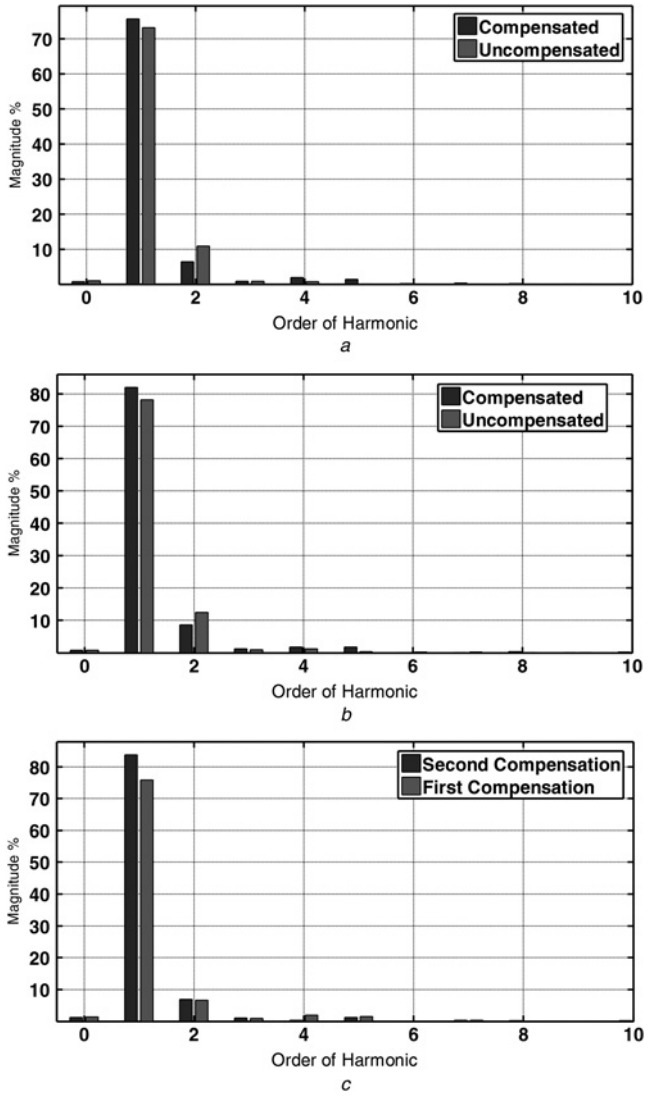

Fig. 11 *Comparing harmonic spectra of the experiments*

a Both uncompensated and compensated relationship (4)
b Both uncompensated and compensated relationship (5)
c Comparing once with twice consecutive compensation

Table 1 Amounts of THDs

NO	Modulation technique	THD % (simulation)	THD % (experimental)
1	relationship (4) ($R_L = 0$)	14.7	14.1
2	relationship (5) ($R_L = 0.05$)	16.5	15.7
3	relationship (4) + SVR	7.1	7.3
4	relationship (5) + SVR	6.7	7
5	relationship (4) + twice SVR	5	4.5

based on the load variations. Here an idea is expressed in order to apply the proposed compensation as an online process. Thus, first the SVR was applied to the implemented boost-inverter for a fixed R_{Load}. Then, different R_{Load} were applied to the proposed offline compensation of Fig. 7, and the resultant duty cycles were

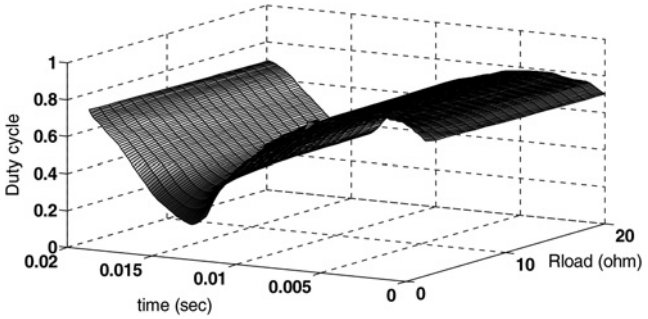

Fig. 12 *Generated duty cycles for one power cycle per phase of the experiments in boost-inverter by varying R_{Load} from 1 to 20 Ω*

stored in a compensating look-up table (CLT). For example, the load resistance R_{Load} was varied from 1 to 20 Ω, where the step size was 1 Ω for the CLT.

The results for one power cycle per phase of the boost-inverter are shown in Fig. 12. Consequently, tracking the load current can be made possible by storing the produced duty cycles on a simple EEPROM or a microcontroller. This is an economical way to mass production of converters.

Ratings of semi-conductor switches limit the maximum nominal load currents depending on different types of power electronic converters. The engaged laboratory test set was designed based on selecting switches that limit the maximum nominal load current to 25 A under 25 V (rms output voltage for each phase). Thus, here the minimum resistance of the load is 1 Ω. Just in case the load has to be < 1 Ω under 25 V, then this implies a bigger load current than 25 A. Hence, the ratings of the switches must be upgraded. Further, a new compensator (lookup table) should be re-run and uploaded to the microcontroller.

6 Conclusion

This paper concentrates on improving the performance of three-phase boost-inverters based on differential connection of DC/DC converters. First, a simple and efficient technique is applied for calculating the pulse widths based on differential connection of converters. Both ideal and non-ideal (considering the resistance of the inductor) are studied in the boost topology. These cases were equipped with the conventional PI-controller to track the rms value of output voltage. Both experiments and simulations show that still the observed waveforms are distorted. To overcome the distortion of waveforms, an SVR-based compensator is proposed to lower the harmonics content. A laboratory prototype of three-phase boost-inverter was designed and implemented in order to verify the performance of the proposed compensation algorithm in addition to the performed simulations. Both simulations and experiments confirm proper performance of the proposed compensating process, in particular, under twice consecutive compensations.

7 References

1 Shen, J.M., Jou, H.L.: 'Transformer-less three-port grid-connected power converter for distribution power generation system with dual renewable energy sources', *IET Power Electron.*, 2012, **5**, (4), pp. 501–509
2 Liang, E.Z., Guo, R., Li, J., Huang, A.Q.: 'A high-efficiency PV module-integrated DC/DC converter for PV energy harvest in

FREEDM systems', *IEEE Trans. Power Electron.*, 2011, **26**, (3), pp. 897–909
3 Yufei, Z., Wenxin, H.: 'Single-stage boost inverter with coupled inductor', *IEEE Trans. Power Electron.*, 2012, **27**, (4), pp. 1885–1893
4 Cecati, C., Ciancetta, F., Siano, P.: 'A multilevel inverter for photovoltaic systems with fuzzy logic control', *IEEE Trans. Ind. Electron.*, 2010, **57**, (12), pp. 4115–4125
5 Cecati, C., Dell'Aquila, A., Liserre, M.: 'A novel three-phase single-stage distributed power inverter', *IEEE Trans. Power Electron.*, 2004, **19**, (5), pp. 1226–1233
6 Erickson, R.W.: '*Fundamentals of power electronics*' (Chapman and Hall, New York, 1997)
7 Chu, G., Chi, K., Tse, R., Chung Wong, S., Tan, S.C.: 'A unified approach for the derivation of robust control for boost PFC converters', *IEEE Trans. Power Electron.*, 2009, **24**, (11), pp. 2531–2544
8 Lu, Z., Sunb, J., Butts, K.R.: 'Linear programming support vector regression with wavelet kernel: a new approach to nonlinear dynamical systems identification', *Math. Comp. Simul.*, 2009, **79**, (7), pp. 2051–2063
9 Viswanathan, K., Orugantiand, R., Srinivasan, D.: 'Nonlinear function controller: a simple alternative to fuzzy logic controller for a power electronic converter', *IEEE Trans. Ind. Electron.*, 2005, **52**, (5), pp. 1439–1448
10 Carrasco, J.M., Galván, E., Valderrama, G.E., Ortega, R., Stankovic, A.M.: 'Analysis and experimentation of nonlinear adaptive controllers for the series resonant converter', *IEEE Trans. Power Electron.*, 2000, **15**, (3), pp. 536–544
11 Mastromauro, R.A., Liserre, M., Asher, G.M., Dell'Aquila, A.: 'Study of the effects of inductor nonlinear behavior on the performance of current controllers for single-phase PV grid converters', *IEEE Trans. Ind. Electron.*, 2008, **55**, (5), pp. 2043–2052
12 Alonge, F., D'Ippolito, F., Raimondi, F.M., Tumminaro, S.: 'Nonlinear modeling of DC/DC convertersusing the Hammerstein's approach', *IEEE Trans. Power Electron.*, 2007, **22**, (4), pp. 1210–1221
13 Qiu, Y., Xu, M., Sun, J., Lee, F.C.: 'A generic high-frequency model for the nonlinearities in buck converters', *IEEE Trans. Power Electron.*, 2007, **22**, (5), pp. 1970–1977
14 Choi, C.H., Cho, K.R., Seok, J.K.: 'Inverter nonlinearity compensation in the presence of current measurement errors and switching device parameter uncertainties', *IEEE Trans. Power Electron.*, 2007, **22**, (2), pp. 576–583
15 Bel Haj Youssef, N., Al-Haddad, K., Kanaan, H.Y.: 'Real-time implementation of a discrete nonlinearity compensating multiloops control technique for a 1.5 kW three- phase/switch/level vienna converter', *IEEE Trans. Ind. Electron.*, 2008, **55**, (3), pp. 1225–1234
16 Guerrero, J.M., Leetmaa, M., Briz, F., Zamarrón, A., Lorenz, R.D.: 'Inverter nonlinearity effects in high-frequency signal-injection-based sensor less control methods', *IEEE Trans. Ind. Appl.*, 2005, **41**, (2), pp. 618–626
17 Zhao, H., Jonathan Wu, Q.M., Kawamura, A.: 'An accurate approach of nonlinearity compensation for VSI inverter output voltage', *IEEE Trans. Power Electron.*, 2004, **19**, (4), pp. 1029–1035
18 Dong, G., Ojo, O.: 'Current regulation in four-leg voltage-source converters', *IEEE Trans. Ind. Electron.*, 2007, **54**, (4), pp. 2095–2105
19 Lee, K.B., Blaabjerg, F.: 'Reduced-order extended luenberger observer based sensorless vector control driven by matrix converter with nonlinearity compensation', *IEEE Trans. Ind. Electron.*, 2006, **53**, (1), pp. 66–75
20 Smola, A.J., Schölkopf, B.: 'A tutorial on support vector regression', *Stat. Comput.*, 2003, **14**, (3), pp. 199–222
21 Vapnik, V.N.: '*The nature of statistical learning theory*' (Springer, 1999)

8 Appendix

8.1 Clarification on obtaining duty cycles in (5)

Since the performance of an ideal DC–DC boost converter can be modelled like a conventional transformer as shown in Fig. 13 [6], it is possible to transfer the primary-side resistance of the DC–DC Boost converter to the secondary-side. Thus, the transformer-like relationship could be developed as below

$$\frac{V_o}{V_{ac}} = \frac{V_o}{V_{in}} \times \frac{V_{in}}{V_{ac}} = a \times \frac{1}{1 + a^2 \dfrac{R_p}{R_{Load}}} \quad a = \frac{n_2}{n_1} = \frac{V_o}{V_{in}} \tag{9}$$

where a is the transformer ratio, V_o and V_{ac} are the secondary and primary voltages, respectively, R_{Load} and R_p are secondary and primary resistances, respectively. Replacing a with $1/(1-D)$ in (9) will result

$$\begin{cases} \dfrac{V_o}{V_{dc}} = \dfrac{V_o}{V_{in}} \times \dfrac{V_{in}}{V_{dc}} = \dfrac{1}{1-D} \times \dfrac{1}{1 + \dfrac{1}{(1-D)^2}\dfrac{R_L}{R_{Load}}} \\ \Rightarrow \dfrac{A\sin(\omega t) + A + V_{dc}}{V_{dc}} = \dfrac{1-D}{(1-D)^2 + \dfrac{R_L}{R_{Load}}} \end{cases} \tag{10}$$

In (10), a second-order equation can be arranged to find D against other parameters, providing the stated relationship in (5).

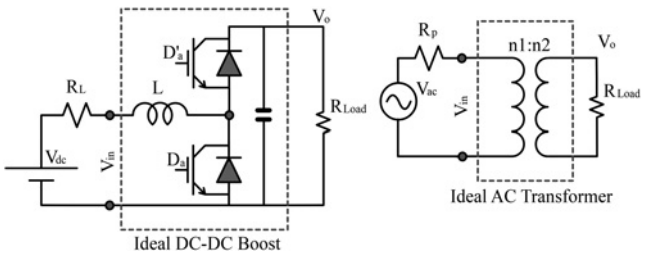

Fig. 13 *Behaviour similarity between DC–DC boost converter and AC transformer*

doi: 10.1049/iet-pel.2013.0046